Kyushu University Global COE Program
Journal of Novel Carbon Resource Sciences, Vol. 3, pp. 21-26, Feb. 2011

Investigation of Liquid Water Behavior in PEFC Porous Media

Yunpeng Fan[*1], Gen Inoue[*2], Yosuke Matsukuma[*2], Masaki Minemoto[*2]
[*1]Graduate School of Engineering, Kyushu University
[*2]Faculty of Engineering, Kyushu University

(Received November 12, 2010; accepted January 21, 2011)

In order to improve the output performance of PEFC, the liquid water has to be removed smoothly from GDL because it prevents gas diffusion. In this study, the relationship between the liquid water distribution and operating condition of fuel cell was examined by experiments with visualized cell and numerical analysis. As a result, it was found that the position and the amount of the liquid water in porous media made a great impact on the output performance. In the case of high temperature but low humidity operating condition, liquid water accumulated near Rib side and caused higher performance.

1. Introduction

Polymer electrolyte fuel cell (PEFC) is a kind of clean energy system that combines hydrogen and oxygen to produce electricity. It is expected as one of most important energy in the next generation due to its high power density, low operating temperature, quick start-up, fast dynamic response and zero emission. Recently, PEFC is widely used in vehicles and stationary cogeneration fields[1)] to solve the energy crisis and environmental problems. As a result, the researches of PEFC are popular now, and various studies focus on the fuel cell design, new applications, alternative catalyst and liquid water management to develop the capability and practical use of PEFC. However, PEFC system is very expensive yet, and the durability is not high enough. One of the approaches to reduce the cost is to decrease the amount of Pt catalyst or to replace the catalyst with other cheaper materials. And another approach is to increase the current density and the output density of single cell. If the output performance of each cell is increased, the number of cells in stack system can be reduced, so the stack cost will drop.

In order to improve the performance of single cell, it is important to speed up the oxygen transfer to catalyst surface in cathode catalyst layer (CL) in the case of high current density condition, because the oxygen transfer rate is dominant[2-3)]. However, the oxygen transfer phenomena in gas diffusion layer (GDL) and micro porous layer (MPL) have not be known and optimized enough. As the principle of PEFC, the fuel cell has to be kept humid to make the proton conductivity of electrolyte membrane high. As a result, in an actual PEFC, liquid water accumulated in GDL during electricity is generated, and the accumulated water prevents the gas diffusion. This is the major reason of the degradation of performance. It is obvious that an efficient way to improve the output performance is to increase the gas diffusion rate of GDL. On the other hand, it is also well recognized that the water condition in porous media makes large influence on the gas diffusion rate. Therefore, in order to improve the output performance, the comprehension of liquid water behavior is extremely necessary.

In this research, the liquid water behavior of GDL surface was investigated with several PEFC visualized cells under different cell temperature and relative humidity conditions. With the experimental data, the relationship between the internal liquid water distribution and the operating condition was considered. In addition, temperature and vapor concentration distribution was calculated by numerical analysis. By comparison between experiment and calculation, the effect of operating condition on vapor concentration distribution was examined.

2. Experiment

2.1 Experimental procedure

Instead of the actual fuel cell, the PEFC visualized single cell (Fig. 1), which was based standard PEFC cell, was used in these experiments. Through the acrylic plate of cell, the behavior of water droplets flowing out from cathode GDL surface in gas channel was observed by digital microscope. This behavior was captured to movie for 30 minutes. At the same time the fluctuation of cell voltage was also measured. From the movies, the flowing points of liquid water were obtained by image processing method which will be explained in next section. The size of cell components is shown in Table 1. The cathode GDL was coated with micro porous layer (MPL) at the catalyst layer side. MPL consists of very small carbon particles with about 1 μm secondary diameter. MPL can reduce contact resistance between MEA and GDL. Fig. 2 shows the visualization experiment apparatus in this study. Hydrogen and oxygen (air) were supplied to visualized cell via humidifier. In PEFC, electrolyte membrane has to be kept humid condition to keep the high proton conductivity. So humidification of supply gas is necessary. And the operating relative humidity can be controlled by the humidifier and thermostat. The cell was set horizontally, and cathode side was set at upper side to observe by microscope. At the back side of anode, rubber heater was set to keep the cell temperature. This temperature was controlled by external thermostat. As the parameter, operating temperature and humidifier temperature were changed. Experimental conditions are shown in Table 2. As a result, the effect of temperature and relative humidity (RH) on liquid water condition was examined.

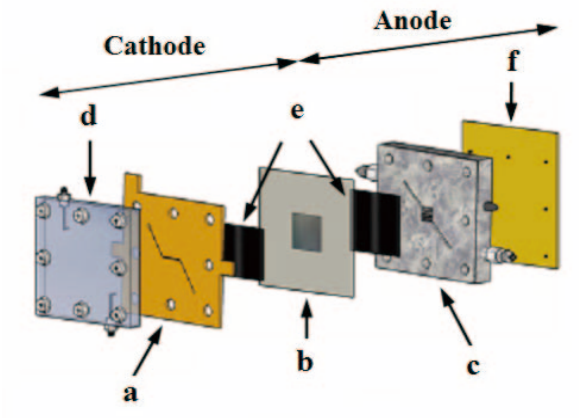

Fig. 1 Structure and components of visualized cell. (a) Separator plated with gold, (b) Membrane electrode assembly (MEA), (c) Gas channel (Graphite), (d) Acrylic plate, (e) Gas diffusion layer (GDL), (e) Back plate

Table 1 Size of cell compone

Part name		Size and amount
Membrane	size:	100 mm×100 mm
	thickness:	30 μm
Electrode	size:	10 mm×10 mm
	Pt content:	0.3 mg/cm^2
Cathode GDL	width:	2 mm, 3 mm, 4 mm
	length:	30 mm
	thickness	190 μm
Anode GDL	size:	10 mm×10 mm
	thickness:	190 μm
Gas channel	width:	1 mm, 2 mm, 3 mm
	depth:	1 mm

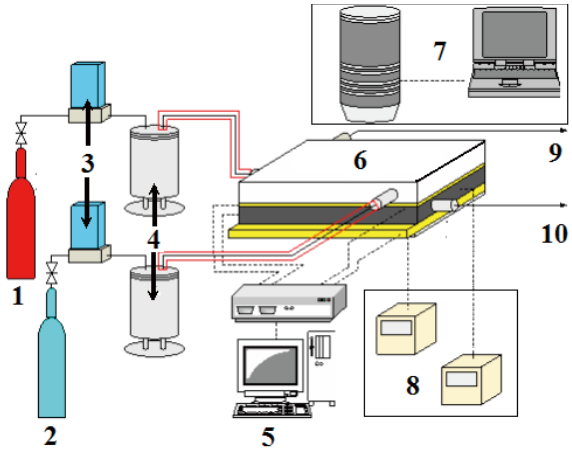

Fig. 2 Visualization experiment apparatus. 1: H_2, 2: Air, 3: Flow control, 4: Humidifier, 5: PC, 6: Cell, 7: Microscope, 8: Thermostat, 9: Air outlet, 10: H_2 outlet

Table 2 Experimental conditions

Factor	Condition
Cell temperature	40 ℃, 50 ℃, 60 ℃
Gas relative humidity	70%, 80%, 90%
Cathode gas component	N_2:79% O_2:21%
Current density	1.0 A/cm^2
H_2 and O_2 utilization ratio	5.4% and 6.4%

2.2 Image processing and data processing

To know the distribution of flowing points of water from GDL, all images of captured movie were changed to binary images by image processing. Next, the droplet parts of each image were extracted by obtaining the difference between initial image and local time image. After this, all images were multiplied, and several clear images of water droplets in gas channel were obtained. Fig. 3 shows the binary image of observation result on GDL surface, the gray part of the photo shows the GDL surface in gas channel, and the bright points on it are the generated water droplets. The other parts of image in black are the ribs of gas channel. After image processing, the clear image of droplet points is obtained and showed in Fig. 4. In these experiments, the section of gas channel was divided to 5 parts from channel center to Rib side. This schematic image of partition of channel is shown in Fig. 5. rib is the solid wall of separator. By counting droplet in each section, the droplets distribution was obtained.

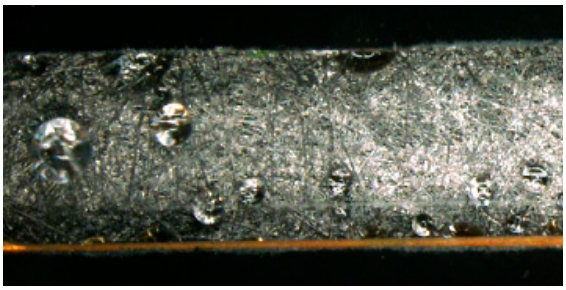

Fig. 3 Observation result of droplets on GDL surface.

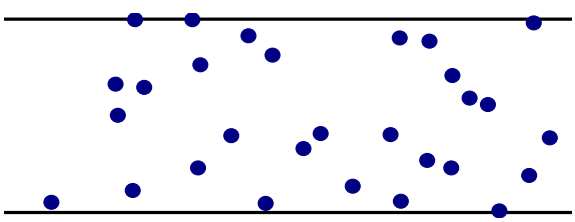

Fig. 4 Points of droplet obtained by image processing.

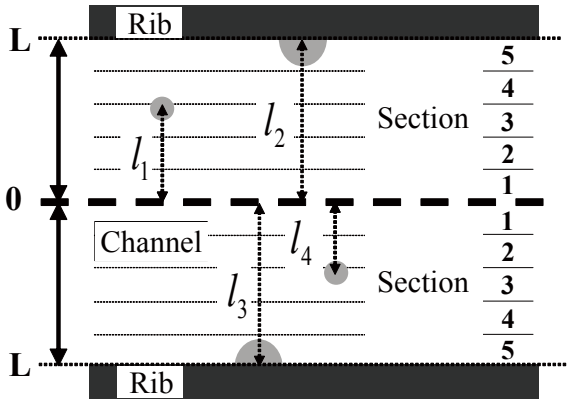

Fig. 5 Schematic image of partition of channel.

2.3 Experimental results

Fig. 6 shows the droplets distribution under different RH conditions. Cell temperature is 50 °C, channel width is 1mm. At rib side (section 5), much droplets flowed out from GDL in the cases of all conditions. Moreover, the amounts of droplets not only at rib side but also at center of channel increased by increasing RH.

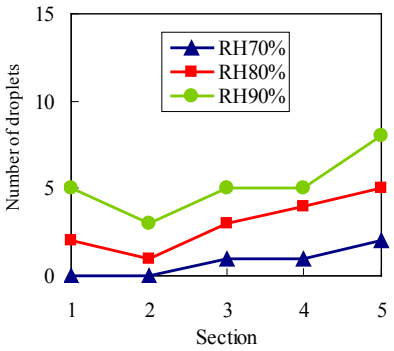

Fig. 6 Droplets distribution at different RH conditions.

Fig. 7 shows the droplets distribution at different temperature condition. Relative humidity is 80%, channel width is 1mm. From this graph, more droplets generated in the case of lower cell temperature. On the other hand, it showed an obvious uneven distribution of generated droplets under high temperature condition.

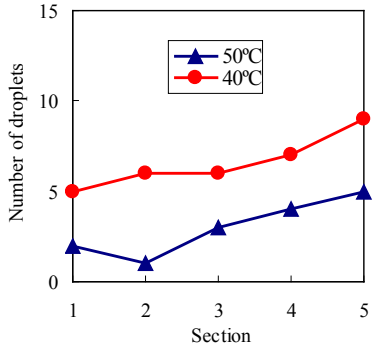

Fig. 7 Droplets distribution at each temperature condition.

Fig. 8 shows the droplets distribution with different channel width. Cell temperature is 40 ºC, relative humidity is 70%. The droplets distribution is more symmetric in narrow gas channel. There was an uneven distribution of generated droplets in wide gas channel.

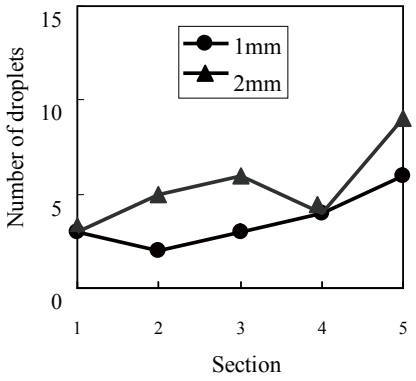

Fig. 8 Droplets distribution with each channel width.

From all of experimental results, generated droplets were less in the center of the channel and increased in the area close to the edge of the rib side. In the case of high temperature and low humidity, much more droplets stayed under rib side. Conversely, in the case of low temperature and high humidity condition, more droplets flowed out GDL surface widely. There was no excessive distribution. With this information, the liquid water condition inside GDL was considered. Fig. 9 shows the inferential image of the liquid water conditions inside and outside GDL by using experimental results. It was guessed that inside liquid water distribution in the direction of in-plane was the same as the droplet distribution observed by these experiments. Next, in order to check the validity of this conjecture, temperature and vapor distribution inside GDL were calculated.

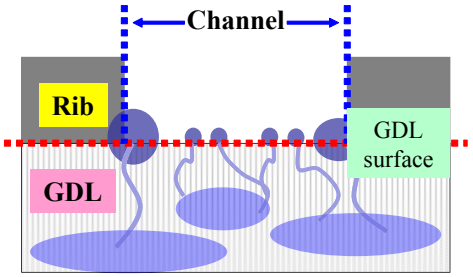

Fig. 9 Liquid water conditions inside and outside GDL.

3. Numerical analysis

3.1 Equations and conditions

In order to explain the experimental results and check the validity of suppositions, the liquid water condition in GDL was examined by numerical analysis. In this calculation, the following assumptions were used. The generated water at catalyst layer is vapor phase only. The temperature and the concentrations at upper surface of

GDL are constant. The gas flow and convection in GDL can be ignored. The effect of liquid water on gas diffusion performance can be ignored. The cell temperature and voltage are kept stable in this system. The diffusions of oxygen and vapor in GDL are assumed as molecular diffusion, and there is only Knudsen diffusion exists in MPL. The schematic image of calculation system and assumptions are showed in Fig. 10. Heat and water are generated in catalyst layer (CL) by cathode oxygen reduction reaction, and then transfer from bottom side to upper side through the GDL and MPL. On the other hand, oxygen diffuses from gas channel to catalyst layer.

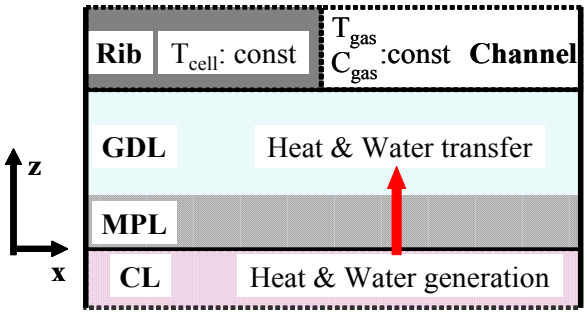

Fig. 10 Schematic image of calculation system and assumptions.

In this calculation, it was assumed that the local temperature and concentration did not affect each other, and these distributions were solved separately by the following equation of energy and mass balance equations.

$$k_x \frac{\partial^2 T}{\partial x^2} + k_z \frac{\partial^2 T}{\partial z^2} = 0 \tag{1}$$

$$D^{eff}_{O_2,x} \frac{\partial^2 C_{O_2}}{\partial x^2} + D^{eff}_{O_2,z} \frac{\partial^2 C_{O_2}}{\partial z^2} = 0 \tag{2}$$

$$D^{eff}_{H_2O,x} \frac{\partial^2 C_{H_2O}}{\partial x^2} + D^{eff}_{H_2O,z} \frac{\partial^2 C_{H_2O}}{\partial z^2} = 0 \tag{3}$$

In these equations, T is temperature, k means the thermal conductivity of GDL and MPL, C is concentration, and D^{eff} means effective diffusion coefficient. Other parameters and their values as D_{O2} and D_{H2O} are showed in Table 3. Subscript O_2 and H_2O mean oxygen and water vapor respectively. As GDL is fibrous porous media, thermal conductivity and effective diffusion coefficient are anisotropic properties. As a result, all the calculations are taken along two directions as show in Fig. 10, and signified in equations as subscript x and z respectively. The effective diffusion coefficients of GDL were obtained by following equations.

$$D^{eff,GDL}_{O_2,d} = \left(\varepsilon_{GDL} / \tau_{GDL,d}\right) D_{O_2} \tag{4}$$

$$D^{eff,GDL}_{H_2O,d} = \left(\varepsilon_{GDL} / \tau_{GDL,d}\right) D_{H_2O} \tag{5}$$

ε means the porosity of porous media, and τ is tortuosity. Subscript d means the direction x or z. The diffusions in MPL were assumed as Knudsen diffusion only, so the diffusion coefficients were calculated as follows.

$$k^{MPL}_x = k^{MPL}_z = k^c (1 - \varepsilon_{MPL}) \tag{6}$$

$$\tau_{MPL} = \varepsilon_{MPL}^{-1/2} \tag{7}$$

$$D^{eff,MPL}_{O_2} = \frac{\varepsilon_{MPL}}{\tau_{MPL}} D^{Kn}_{O_2}, \quad D^{Kn}_{O_2} = \frac{2}{3} r \sqrt{\frac{8RT}{\pi M_{O_2}}} \tag{8}$$

$$D^{eff,MPL}_{H_2O} = \frac{\varepsilon_{MPL}}{\tau_{MPL}} D^{Kn}_{H_2O}, \quad D^{Kn}_{H_2O} = \frac{2}{3} r \sqrt{\frac{8RT}{\pi M_{H_2O}}} \tag{9}$$

Table 3 Calculation conditions

Parameter		Value
Operating conditions		
Cell temperature(T_{cell})		40, 50 ℃
Relative humidity(RH)		70, 90 %
Average current density(i)		1.0 A/cm^2
Components		
GDL	porosity(ε_{GDL})	0.78
	thickness(-)	170 μm
	tortuosity	
	X direction($\tau_{GDL,x}$)	1.205
	Z direction ($\tau_{GDL,z}$)	1.343
	thermal conductivity	
	X direction(k_x)	21.0 W/(m・K)
	Z direction (k_z)	1.7 W/(m・K)
MPL	porosity(ε_{MPL})	0.2
	thickness(-)	30 μm
	pores' average radius(r)	1.0×10^{-7} m
MEA	thickness(t_m)	30 μm
Channel	width	0.5 mm
Rib	width	0.5 mm
Coefficients		
O_2 diffusion coefficient(D_{O2})		2.350×10^{-5} m^2/s
H_2O diffusion coefficient(D_{H2O})		2.505×10^{-5} m^2/s
Voltage (overall enthalpy) (E_{max})		1.481 V
Electromotive Force (E^0)		1.23 V
Gas constant(R)		8.314 J/(mol・K)
Faraday constant(F)		96485.309 C/mol
Transfer coefficient(α_t)		0.3
Thermal conductivity of carbon black (k^c)		98.0 W/(m・K)

MPL is made by micro carbon particles, so the thermal conductivities and effective diffusion coefficient of all the directions are the same. k^c is the thermal conductivity of carbon black. Bruggeman equation (7) shows the relationship between the tortuosity and porosity of MPL[4]. D^{Kn} means the Knudsen diffusion coefficient, r is the average radius of pores in MPL, R means gas constant, and M is the molecular weight.

At the upper side of GDL, the boundary condition at gas channel part and rib part are not same. Each condition is showed as follows.

$$\text{(Channel)} \quad T=T_{gas},\ C_{O_2} = C^{gas}_{O_2},\ C_{H_2O} = C^{gas}_{H_2O} \tag{10}$$

$$\text{(Rib)} \quad T=T_{cell},\ \frac{\partial C_{O_2}}{\partial z} = 0,\ \frac{\partial C_{H_2O}}{\partial z} = 0 \tag{11}$$

At right and left side in Fig. 10, wall condition was used as the boundary condition in order to calculate temperature and concentration distributions. As a result, the boundary conditions of CL-MPL surface were set with the following equations[5].

$$k_z^{MPL}\frac{\partial T}{\partial z} = (E_{Max} - V_{cell})i \tag{12}$$

$$D_{O_2,z}^{eff,MPL}\frac{\partial C_{O_2}}{\partial z} = -\frac{i}{4F} \tag{13}$$

$$D_{H_2O,z}^{eff,MPL}\frac{\partial C_{H_2O}}{\partial z} = (1+2\alpha)\frac{i}{2F} \tag{14}$$

E_{Max} means the voltage value estimated by enthalpy change of overall reaction, V_{cell} means cell voltage, i is the local current density, F is the Faraday's constant, α is net water transfer coefficient in membrane, and superscript MPL means the value of MPL near CL. Cell voltage was calculated by the following Butler-Volmer equation.

$$V_{cell} = E - \frac{RT_{cell}}{\alpha_t 2F}\ln\left(\frac{iC_{O_2}^{ref}}{i_{O_2}^{ex}C_{O_2}^{e}}\right) - R_{ohm}i \tag{15}$$

In this equation, E means effective motive force of overall reaction, α_t is transfer coefficient of cathode electrode reaction, C^{ref} is reference concentration, i^{ex} is exchange current density, C^e is local concentration of catalyst layer surface, and R_{ohm} means membrane ohmic resistance. The values of these coefficients were calculated by the method from other paper[6]. Net water transfer coefficient was calculated by electro-osmotic effect and back diffusion as follows[6].

$$\alpha = n_d - \frac{F}{i}D_{H_2O}^{m}\frac{C_{H_2O}^{c(m)} - C_{H_2O}^{a(m)}}{t_m} \tag{16}$$

n_d means the electro-osmotic coefficient, $C^{c(m)}$ and $C^{a(m)}$ mean the concentration of membrane surface in cathode side and anode side respectively, and D^m is the water effective diffusion coefficient inside membrane. The values of n_d and D^m are also obtained by other papers[6,7]. The calculation conditions and parameters are shown in Table 3. Furthermore, the vapor condensation part was examined with local temperature and vapor concentration distribution. In this study, the difference between the local vapor partial pressure and the saturated vapor pressure was calculated as Δp_{vapor}. Saturated vapor pressure was calculated with local temperature. Vapor is easy to condense at the position which the Δp_{vapor} value is high. In this study, the effect of liquid water on gas diffusion and heat transfer was ignored.

3.2 Calculation results

Fig. 11 shows the vapor concentration distribution when the RH is 90%, cell temperature is 50 °C and cell voltage is 0.5 V. Upper graph is two-dimensional distribution, and lower graph is vapor concentration distribution in the direction of in-plane at each slice. In these figures, it was found that vapor concentration was higher at under rib area because the diffusion length under Rib is longer than that under channel. So diffusion rate at this part decreased and vapor accumulated here more easily.

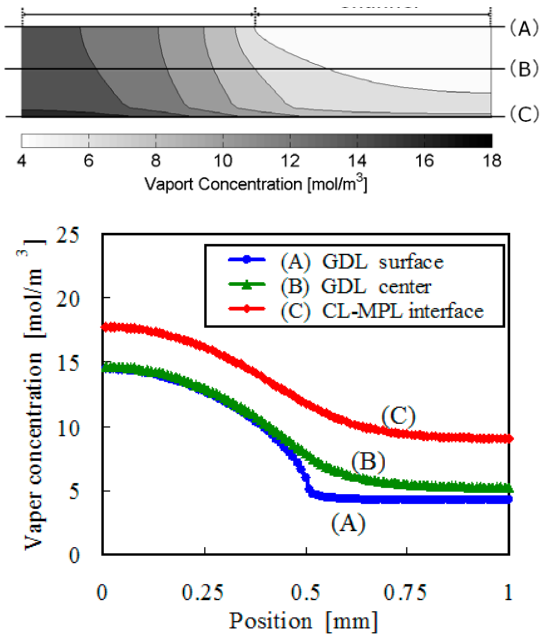

Fig. 11 Vapor concentration distribution in GDL.

Fig. 12 shows the temperature distribution at the same condition as Fig. 11. The temperature of catalyst layer increased by generated heat of overvoltage. In particular, current density under gas channel was higher than that of other parts because of the high oxygen diffusion rate. So the temperature at center of gas channel on the interface of catalyst layer and MPL was the highest. On the other hand, the temperature under rib on the GDL surface was the lowest because it attached cold solid wall. Moreover, though GDL has only 200 μm thickness, there were about 1.5 °C differences inside GDL.

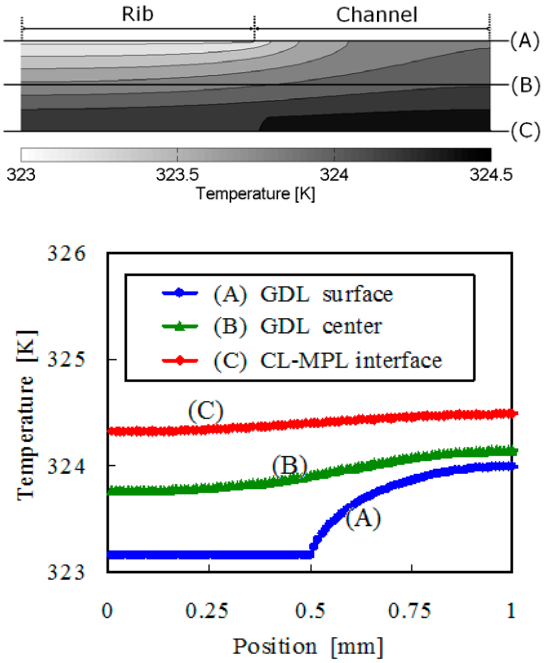

Fig. 12 Temperature distribution in GDL.

Fig. 13 shows the vapor condensation distribution with Δp_{vapor} under each operating condition. In these figures,

white parts mean the value of Δp_{vapor} is negative and the vapor doesn't condense there. From these graphs, in all the cases, vapor is easy to condense under rib.

Comparing with (a) and (c) of Fig. 13, it can be confirmed that the condensation part under channel increased by increasing RH. Similarly comparing with (b) and (c) it can be confirmed that the condensation part under channel increased by increasing cell temperature. Therefore, these distributions of temperature and vapor concentration strongly affect liquid water behavior in GDL. In addition, the experimental results of droplets distribution on GDL surface and the calculation results of vapor condensation part inside GDL were almost the same qualitatively.

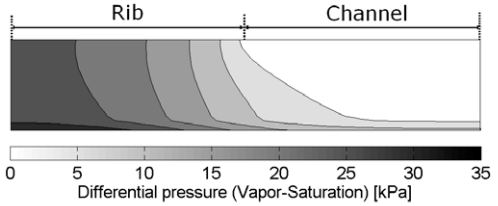

(a) Cell temperature 50 ºC, RH 90%

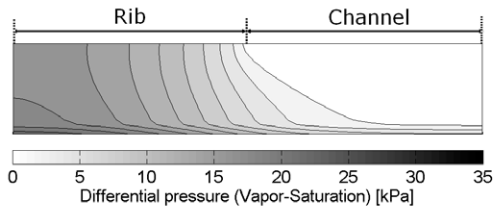

(b) Cell temperature 40 ºC, RH 70%

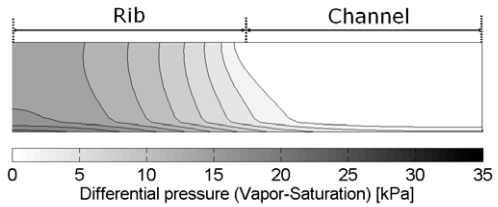

(c) Cell temperature 50 ºC, RH 70%

Fig. 13 Δp_{water} distributions in GDL under different temperature and humidity conditions.

4. Conclusions

In this study, the generated droplets distributions on GDL surface were observed with visualized polymer electrolyte fuel cell during electricity generated under different conditions. In addition, the vapor condensation distribution was examined by heat and mass transfer calculation in GDL. Results showed the cell temperature, relative humidity and the width of gas channel strongly affected the liquid water distribution in GDL. Especially, in the case of high temperature and low humidity, much more droplets stayed under rib side. The experimental results of droplets distribution on GDL surface and the calculation results of vapor condensation part were almost same qualitatively. This distribution can be controlled by operating condition in order to improve gas diffusion rate in two-phase porous media. And this knowledge can be applied to improve PEFC output performance and to reduce the stack cost.

In our future study, to know the effect of other factor on gas diffusion performance in two-phase condition, experimental method and calculation model have to be improved with other devise and with other equations.

Acknowledgement: This research was financially supported by PEFC program of new energy and industrial technology development organization (NEDO), Japan.

References

1) C. Siegel, *Energy*, **33**, 1331 (2008).
2) G. Inoue, Y. Matsukuma, M. Minemoto, *ECS Trans.*, **16**(2), 769 (2008).
3) L. Zhang, Y. Liu, H. Song, S. Wang, Y. Zhou, S. J. Hu, *J. Power. Soc.*, **162**(2), 1165 (2006).
4) A. Z. Weber, J. Newman, *J.Electrochem.Soc.*, **152**(4), A677 (2005).
5) J. S. Yi, Trung V. Nguyen, *J. Electrochem. Soc.*, **146**(1), 38 (1999).
6) T. V. Nguyen, R. E. White, *J. Electrochem. Soc.*, **140**(8), 2178 (1993).
7) A. Parthasarathy, S. Srinivasan, A. J. Appleby, C. R. Martin, *J. Electrochem. Soc.*, **139**(9), 2530 (1992).